

FOREIGN GAS BROADENING OF LINES
IN THE WINGS OF THE CO FUNDAMENTAL

by 45

DAVID EDWARD SCHMIEDER

B.S., Wisconsin State University - Platteville, 1967

A MASTER'S THESIS

submitted in partial fulfillment of the
requirements for the degree


MASTER OF SCIENCE

Department of Physics

KANSAS STATE UNIVERSITY

Manhattan, Kansas
1969

Approved by


Major Professor

LD
2668
T4
1969
S35

ii

TABLE OF CONTENTS

List of Figures	iii
List of Tables	v
I. INTRODUCTION	1
II. THEORY OF ABSORPTION LINE SHAPES	5
A. Lambert's Law	5
B. Line Width	6
III. RELATIVE BROADENING ABILITIES	17
IV. REVIEW OF PREVIOUS WORK	22
V. EXPERIMENTAL RESULTS	31
A. Problem for Investigation	31
B. Description of Equipment and Experimental Procedure	31
C. Discussion of Results	44
APPENDIX	71
A. Validity of Theoretical Assumptions and Approximations	71
B. Sources and Treatment of Experimental Error	71
ACKNOWLEDGEMENT	77
REFERENCES	78
ABSTRACT	

LIST OF FIGURES

Figure number

1	Energy level diagram	4
2	Illustration of the effect of Lambert's Law	5
3	Amplitude-time curve of damped oscillator	7
4	Comparison of Lorentz and Maxwellian line shapes	11
5	Infinite wavetrain associated with undamped oscillatory motion	13
6	Frequency distribution of undamped wave	13
7	Wave truncated by collisions	13
8	(a) Frequency distribution of truncated wave versus electric field intensity $\mathcal{E}(v)$ (b) Frequency distribution of truncated wave versus $ \mathcal{E}(v) ^2$	14
9	Typical curves of growth	24
10	Experimental F values of H_2 determined by Draegert and Williams	28
11	Experimental F values of Ar and He determined by Draegert and Williams	30
12	Schematic diagram of entire apparatus	33
13	Typical spectra of CO fundamental	38
14	Actual size tracing of typical spectra for lines m 14	40
15	Actual size tracing of typical spectra for lines m 19	43
16	Experimental F values of H_2 from Set I and Set II	49
17	Experimental F values of D_2 from Set I and Set II	51
18	Experimental F values of He from Set I and Set II	53
19	Experimental F values of Ar from Set I and Set II	55
20	Composite plot of F values for H_2	59
21	Composite plot of F values for D_2	61
22	Composite plot of F values for He	63
23	Composite plot of F values for Ar	65

Figure number

24	Chai's experimental B values	68
25	Illustration of uncertainty propagation	74

LIST OF TABLES

Table number

I	Half-widths $\gamma_{c,b}^{\circ}$ for lines $0 < m < 20$ in the CO fundamental	26
II	F values for He, Ar, H ₂ , and D ₂ from Set I and Set II	45
III	Composite F values for He, Ar, H ₂ , and D ₂	56
IV	Half-widths $\gamma_{c,b}^{\circ}$ for lines $15 < m < 29$ in the CO fundamental	70

I. INTRODUCTION

Much information of scientific and technical value can be gained by studies of the transmission of infrared radiation by atmospheric gases. First, a detailed knowledge of the emission and absorption processes can yield information concerning molecular structure and intermolecular forces. Secondly, infrared studies provide information of prime importance in studies of the earth's "heat balance." Radiant flux from the sun, which can be regarded as a 6000° K black body, must pass through the atmosphere to reach the earth's surface; some of this radiation in the ultraviolet and infrared region of the spectrum is selectively absorbed in the atmosphere. Radiant flux from the earth's surface, which can be regarded as a 300° K black body, must pass through the atmosphere on its way into space; again, some of this infrared radiation is selectively absorbed in the earth's atmosphere. Some of the absorbed radiation is immediately re-emitted and the remainder serves to raise the temperature of the atmosphere. Finally, a detailed knowledge of atmospheric absorption is necessary for proper design of infrared scanning systems.

The polyatomic gases H_2O , CO_2 , O_3 , N_2O , Cl_4 , and the polar diatomic gas CO absorb strongly in the infrared. The homopolar atmospheric constituents H_2 , N_2 , D_2 , and O_2 as well as the noble gases do not absorb in the infrared but have an influence on the ability of the other gases to absorb.

Since the absorption and emission of infrared electromagnetic radiation in the earth's atmosphere involves many uncontrollable parameters, laboratory studies of synthetic atmospheres are necessary. The present study

involves measurements of the influence of H_2 , D_2 , He, and Ar on the absorption of carbon monoxide in the region of its fundamental vibration-rotation band.¹ The transitions involved in this band are indicated in the energy level diagram in Fig. 1.



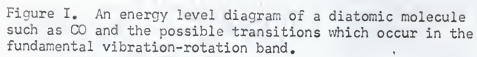
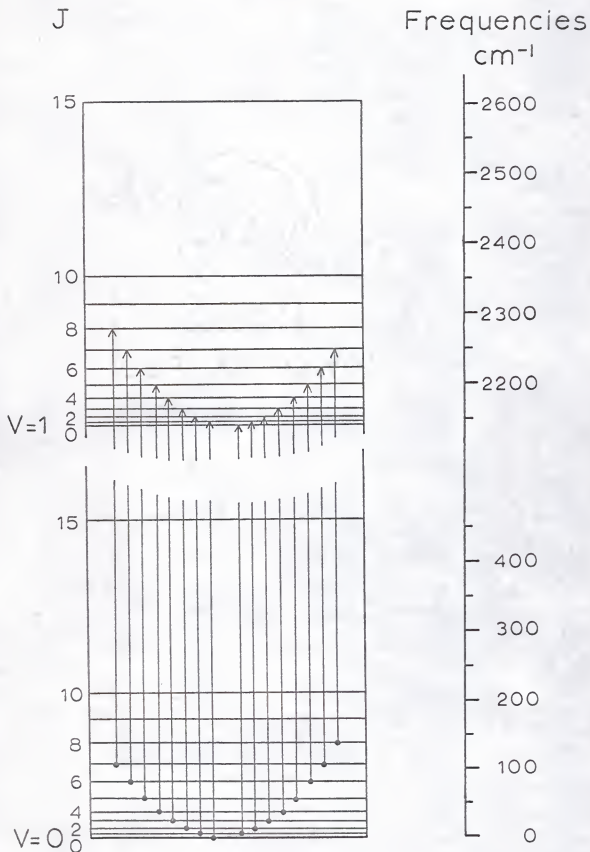


Figure I. An energy level diagram of a diatomic molecule such as CO and the possible transitions which occur in the fundamental vibration-rotation band.



II. THEORY OF ABSORPTION LINE SHAPES

A. Lambert's Law

When an infrared beam encounters a homogeneous absorbing medium such as the sample in the absorption cell shown in Fig. 2, it is possible that part

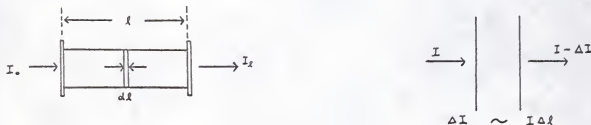


Fig. 2

of the beam will be absorbed. Lambert assumed that the beam experienced an intensity decrease dI in passing through thickness $d\ell$ and that dI was proportional to I and to $d\ell$ as suggested in Fig. 2. By introducing proportionality constant K , Lambert wrote the differential equation

$$dI = -KI d\ell,$$

which may be solved to give

$$I = I_0 e^{-K\ell},$$

where I_0 is the intensity of the incident beam and I is the intensity of the emerging beam. The transmittance T of the sample is defined as the ratio I/I_0 ; thus $T = e^{-K\ell}$. The absorptance A is defined as the ratio $(I_0 - I)/I_0$; thus $A = 1 - e^{-K\ell}$.

Recognizing that absorption is an atomic or molecular process, Beer assumed that quantity $K\ell$ was proportional to the number of absorbers per unit cross-section of the beam; thus

$$T = e^{-kn\ell},$$

where n is the number of absorbers per unit volume and k is a molecular

absorption coefficient. The quantity $n\ell$ is referred to as the optical density, absorber thickness, or absorber concentration.

Atmospheric absorption is quite selective. The absorption coefficient k is frequency-dependent; consequently, the absorptance A and transmittance T are frequency-dependent and any expression of these terms should clearly show their dependence on frequency ν . Hence, the spectral transmittance $T(\nu)$ is usually written

$$T(\nu) = e^{-k(\nu)n\ell}$$

and the spectral absorptance $A(\nu)$ is written

$$A(\nu) = 1 - e^{-k(\nu)n\ell}.$$

The spectral absorption coefficient $k(\nu)$ for gases in the infrared is a rapidly varying function of frequency. Each transition shown in Fig. 1 constitutes an absorption line. It has been shown that $k(\nu)$ for each line can be approximated by the Lorentz expression

$$k(\nu) = \frac{S}{\pi} \frac{\gamma}{(\nu_0 - \nu)^2 + \gamma^2}, \quad (1)$$

where the line strength $S = \int_0^\infty k(\nu) d\nu$ is directly proportional to the quantum mechanical transition probability and depends on the difference in the populations of the initial and final energy states; ν_0 is the central frequency of the line, and γ is the half-width of the line at half maximum.

B. Line Width

As indicated in Eq. (1), the spectral absorption coefficient $k(\nu)$ is not a δ -function centered at ν_0 . Radiation absorbed or emitted by molecules does not consist of perfectly monochromatic radiation of frequency ν_0 but involves a "band" of frequencies centered at ν_0 . The finite width of this

band is related to γ . The factors contributing to line width are (1) natural line broadening, (2) Doppler broadening, and (3) collision broadening, each of which will be discussed briefly.

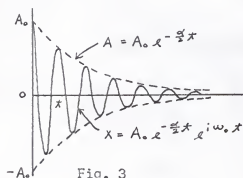
Natural line broadening can be discussed from both a classical and a quantum mechanical viewpoint. According to classical electromagnetic theory² the motion of a radiating oscillator is continually damped by loss of energy to the electromagnetic field; that is to say, the principle of energy conservation requires that the energy gained by the electromagnetic field must be equal to the energy lost by the oscillator as its amplitude decreases. The energy E of such an oscillator at time t can be expressed in the form

$$E = E_0 e^{-\alpha t},$$

where E_0 is the initial energy, t is the time, and α is called the relaxation constant. Since the energy of an oscillator is proportional to the square of the amplitude A , the amplitude can be written $A = A_0 e^{-\frac{\alpha}{2}t}$, and the displacement x of the oscillator at any time t can be written

$$x = A_0 e^{-\frac{\alpha}{2}t} e^{i 2\pi\nu_0 t},$$

where A_0 is the initial displacement. Fig. 3 illustrates an amplitude-time curve of such a damped oscillator.



The electric field \mathcal{E} associated with electromagnetic waves emitted by such an oscillator decreases with t in the same way as the amplitude of the oscillator, so that the electric field \mathcal{E} is given by

$$\mathcal{E} = \mathcal{E}_0 e^{-\frac{\alpha}{2}t} e^{i2\pi\nu_0 t},$$

where \mathcal{E}_0 is the initial value of the electric field. This equation is not associated with a monochromatic wave of frequency ν_0 but with a set of waves with frequencies ν in the vicinity of ν_0 .

An ordinary Fourier analysis of the damped wave emitted by the oscillator gives for the spectral intensity as a function of frequency

$$I(\nu) = (\text{constant}) \frac{\alpha}{2\pi} \frac{1}{4\pi^2(\nu - \nu_0)^2 + \left(\frac{\alpha}{2}\right)^2}. \quad (2)$$

When ν equals ν_0 , the spectral intensity $I(\nu)$ takes its maximum value.

Likewise, when $4\pi^2(\nu - \nu_0)^2 = \left(\frac{\alpha}{2}\right)^2$ the intensity has a value equal to half its value at maximum; thus $\nu - \nu_0 = \frac{\alpha}{4\pi}$ where $\frac{\alpha}{4\pi}$ is now the natural line half-width γ_n . Hence, it can be seen that Eq. (2), which results from a consideration of power emitted, is of the same form as Eq. (1) which results from a consideration of power absorbed. This is to be expected since Kirchhoff's Law demands that the ratio of the emitted power to the absorbed power for radiation of the same frequency be a constant for all bodies at the same temperature.

Natural line broadening can also be discussed from the quantum mechanical viewpoint. According to quantum mechanical principles, the actual energy of a molecule in a given state E is not to be thought of as associated with a level of zero width. Heisenberg's uncertainty principle, $\Delta E \Delta t \sim \hbar$, establishes ΔE as the uncertainty in the energy of a molecule in state E where Δt is the lifetime of a molecule in the state, and \hbar is Planck's

constant divided by 2π . For a collection of molecules in state E, the mean width $\overline{\Delta E}$ of the level is related to the mean lifetime τ of a molecule in the state; thus

$$\overline{\Delta E} \sim \frac{\hbar}{\tau} .$$

This implies that the greater the mean life of a molecule in a given state, the smaller will be the breadth $\overline{\Delta E}$ of the energy level.

As indicated in Fig. 1, absorption involves radiative transitions from lower to higher energy states. The width $\Delta\nu$ of an absorption line is therefore related to the finite widths ΔE of the initial and final energy states; i.e.,

$$\Delta\nu = \frac{\Delta E}{h} \sim \frac{\hbar}{\Delta t h} = \frac{1}{2\pi \Delta t} .$$

For a collection of molecules, the mean width $\overline{\Delta\nu}$ is given by the expression

$$\overline{\Delta\nu} \sim \frac{1}{2\pi \tau} .$$

If the mean width $\overline{\Delta\nu}$ is identified with the half-width γ_n of an absorption line,

$$\gamma_n = \frac{1}{2\pi \tau} , \quad (3)$$

where τ is related to the mean lifetime of the molecules in the initial and final states. Thus, from the quantum mechanical viewpoint, the natural width, $\gamma_n = \frac{1}{2\pi \tau}$, of a spectral line depends upon the lifetimes of a molecule in the initial and final state involved in the transition.

In order to establish a connection with the classical value, $\gamma_n = \frac{\alpha}{4\pi}$, in which α can be determined from classical principles, the quantum mechanical half-width $\gamma_{n_{j \rightarrow i, \tau}}$ is sometimes written³

$$\gamma_{n_{j \rightarrow i, \tau}} = f_{ij} \gamma_{n_{\text{class}}} ,$$

where f_{ij} is the "oscillator strength" of the transition from state i to state j. Although $\gamma_{n_{j \rightarrow i, \tau}}$ is different for molecules in different levels,

it is of the same order of magnitude as that given by the classical theory of radiation damping.

It is usual to express the half-width in terms of wavenumbers:

$\gamma_n = (2\pi c \tau)^{-1}$. The mean lifetime for an excited state in the infrared is approximately 10^{-4} sec. Thus the natural line breadth is on the order of $5 \times 10^{-8} \text{ cm}^{-1}$, which is a very small quantity compared with the spectrometer slitwidth, which is on the order of 1.0 cm^{-1} .

The second cause of line width is the Doppler effect. Owing to thermal motion, emitting and absorbing molecules are moving in various directions relative to a frequency measuring instrument. Consequently, if the effect of natural line broadening is negligible, radiation measured from the emitting molecules is not monochromatic because of Doppler frequency shifts.

The measured frequency ν for radiation received from a molecule having a velocity component u_x in a coordinate system in which the observer is at rest and the x-axis constitutes his "line-of-sight" is given by⁴

$$\nu = \frac{u_x}{c} \nu_0 + \nu_0,$$

which implies that

$$u_x = \frac{c}{\nu_0} (\nu - \nu_0), \quad (4)$$

where ν_0 is the frequency for a molecule with a zero x-component of velocity and c is the speed of light.

The spectral intensity $I(\nu)$ measured for emissions from molecules moving with their x-components of velocity in the range between u_x and $u_x + du_x$ is proportional to the mean number of molecules with velocity components between u_x and $u_x + du_x$. Furthermore, the probability⁵ that a molecule in a gas at temperature T will have an x-component of velocity between u_x and $u_x + du_x$ is proportional to $\exp(-mu_x^2/2kT)$, where \mathcal{L}

is Boltzmann's constant. Thus, if u_x is written in terms of the frequency shift $(v - v_0)$ as shown in Eq. (4), it follows that

$$I(v) = (\text{constant}) e^{-\frac{m c^2}{2 k T} \left(\frac{v - v_0}{v_0} \right)^2} \quad (5)$$

Hence, the Doppler effect produces a frequency spread in the shape of a Maxwellian velocity distribution which has its maximum value at $v = v_0$ and half-width γ_d at half maximum of

$$\gamma_d = v - v_0 = \frac{v_0}{c} \sqrt{\frac{2 k T}{m} \ln 2} \quad ,$$

which is on the order of 10^{-3} cm^{-1} at room temperature. This is a far larger half-width than that associated with natural line broadening, but is smaller than the spectral slitwidths of most spectrometers.

In comparing the line shape given by the Maxwellian distribution with that given by the Lorentz expression of Eq. (2) for natural line broadening, both expressions reduce to the form

$$I(v) = A - B(v - v_0)^2 \quad ,$$

where A and B are constants, provided $(v - v_0)$ is small. The Maxwellian expression for Doppler broadening is exponential and therefore decreases rapidly with increasing magnitude of $(v - v_0)$. On the other hand, the Lorentz distribution for natural line broadening decreases slowly with $(v - v_0)$; thus in regions remote from the center, the Lorentz expression provides a larger contribution, as illustrated⁶ in Fig. 4.

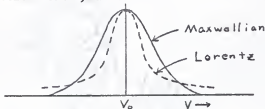


Fig. 4

The derivation given above for Eq. (5) is based on classical considerations. Heitler⁷ has given a derivation involving the transformation properties of a light quantum under a Lorentz transformation which are the same as those for the total momentum and energy of a particle.

The spectral absorption coefficient $k(\nu)$ for Doppler-broadened lines can be written in the same Maxwellian form,

$$k(\nu) = (\text{Constant}) e^{-\frac{m c^2}{2 k T} \left(\frac{\nu - \nu_0}{\nu_0} \right)^2},$$

since Kirchoff's Law establishes a balance between spectral power emission and power absorption for every frequency interval by a body at a given temperature.

Collision broadening, having an approximate half-width of 0.1 cm^{-1} for one atmosphere of pressure, is the most significant broadening effect in the present study and is so much greater than either natural or Doppler broadening that the latter two effects can be ignored in comparison.

The expression of undamped oscillatory motion of displacement A at time t and frequency ν_0 for a molecule is

$$A = A_0 e^{-i 2\pi \nu_0 t},$$

where A_0 is the amplitude. Associated with this motion, as with the oscillator discussed for radiation damping, is an electric field amplitude \mathcal{E} which varies with time in the same way as the mechanical amplitude and is thus given by

$$\mathcal{E}(t) = \mathcal{E}_0 e^{-i 2\pi \nu_0 t},$$

where \mathcal{E}_0 is the amplitude of the electric field.

The wavetrain associated with the molecule will extend over all time, as shown in Fig. 5.



Fig. 5

The associated electromagnetic wave will be monochromatic as can be seen by an examination of the spectral electric field frequency distribution $\mathcal{E}(\nu)$, which can be written in terms of a Fourier transform as

$$\mathcal{E}(\nu) = \frac{1}{\sqrt{2\pi}} \int_{-\infty}^{+\infty} \mathcal{E}(x) e^{2\pi i \nu x} dx .$$

Then $\mathcal{E}(\nu)$ is given by the delta function

$$\mathcal{E}(\nu) = \mathcal{E}_0 \sqrt{2\pi} \delta(\nu - \nu_0) .$$

Hence the only frequency for which the electric field has a value is at $\nu = \nu_0$, as shown in Fig. 6, where $\mathcal{E}(\nu_0)$ is infinite.

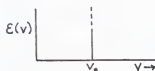


Fig. 6

If the oscillating molecule emitting this monochromatic wave has its radiating process interrupted by collisions with other molecules at time intervals $\Delta x = \Gamma$, the wave will no longer be infinite. A collision has the effect of truncating the wave as suggested in Fig. 7.

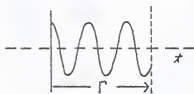


Fig. 7

That a truncated wave like that in Fig. 7 is not monochromatic can be shown

by an examination of the frequency distribution by using again the Fourier transform

$$\mathcal{E}(\nu) = \frac{1}{\sqrt{2\pi}} \int_0^{\Gamma} \mathcal{E}(t) e^{2\pi i \nu t} dt = \frac{\mathcal{E}_0}{\sqrt{2\pi}} \int_0^{\Gamma} e^{2\pi i (\nu - \nu_0) t} dt .$$

Thus

$$\mathcal{E}(\nu) = \frac{\mathcal{E}_0}{\sqrt{2\pi}} \frac{e^{2\pi i (\nu - \nu_0) \Gamma} - 1}{2\pi i (\nu - \nu_0)} ,$$

where it is understood here that only the real part has significance. The resulting frequency distribution is no longer a delta function, but instead displays a frequency spread about ν_0 as suggested in Fig. 8-a.

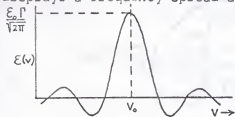


Fig. 8-a

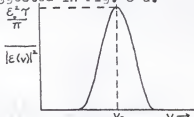


Fig. 8-b

The wave, subject to interruptions at time intervals Γ , has a spectral intensity distribution $I(\nu)$ which is proportional to $|\mathcal{E}(\nu)|^2$ averaged over all values of Γ , or $I(\nu) \propto \overline{|\mathcal{E}(\nu)|^2}$. To develop an expression for $\overline{|\mathcal{E}(\nu)|^2}$, let $P(\tau) d\tau$ equal the probability that a molecule, after surviving without collisions for a time τ , suffers a collision in the time interval between τ and $\tau + d\tau$. Then $P(\tau) d\tau$ is given⁸ by the expression

$$P(\tau) d\tau = \frac{e^{-\tau/\bar{\tau}}}{\bar{\tau}} d\tau ,$$

where $\bar{\tau} = \tau$ the mean time between collisions, the "collision time" or "relaxation time" of the molecule. Then it follows that $\overline{|\mathcal{E}(\nu)|^2}$ must be given by the expression

$$\overline{|\mathcal{E}(\nu)|^2} = \int_0^{\infty} \frac{e^{-\tau/\bar{\tau}}}{\bar{\tau}} |\mathcal{E}(\nu)|^2 d\tau ,$$

which implies that

$$|\mathcal{E}(v)|^2 = \frac{\mathcal{E}_0^2}{4\pi^3} \frac{1}{(v-v_0)^2 + \left(\frac{1}{2\pi\tau}\right)^2}$$

A plot of this function is shown in Fig. 8-b. Thus, the spectral intensity distribution $I(v)$ for the radiating molecule, in a form similar to Eq. (2), can be written

$$I(v) = I_0 \frac{\frac{1}{2\pi\tau}}{(v-v_0)^2 + \left(\frac{1}{2\pi\tau}\right)^2},$$

where I_0 is the constant of proportionality and, in analogy to Eq. (2), $\frac{1}{2\pi\tau}$ equals the line half-width γ .

However, it is likely that a gas will not have just one, but many, molecules emitting radiation during various time intervals. It is necessary to define a mean time between collisions τ_c for the entire system of molecules; then

$$\frac{1}{2\pi\tau_c} = \gamma_c \quad (6)$$

Again, Kirchoff's law establishes a balance between emission and absorption; thus, the spectral absorption coefficient $k(v)$ for the system can be written

$$k(v) = \frac{S}{\pi} \frac{\gamma_c}{(v-v_0)^2 + \gamma_c^2},$$

where, as in Eq. (1), the line strength S equals $\int_0^\infty k(v)dv$.

Just as the natural line broadening process can be discussed from a quantum mechanical viewpoint, so also can the collision broadening process. For collision broadening, the uncertainty relation $\Delta E \Delta t \sim \hbar$ establishes ΔE as the uncertainty in the energy of a state E . This energy state E of a molecule depends upon the perturbing influence of a collision. As a molecule approaches the emitting molecule in the collision process, certain intermolecular forces⁹ can produce a change in the energy of excited states associated with the emitting molecule. This can change the frequency of the emitting molecule and result in line broadening. The quantity Δt is

established as the duration of the unperturbed energy states of the isolated molecule, the time interval between collisions.

For an ensemble of molecules, the mean time τ_c between collisions is also the mean duration of the discrete energy levels E of isolated molecules. The energy breadth of each level is given by $\Delta E \cdot \tau_c \sim \hbar$ or $\Delta E \sim \hbar / 2\pi \tau_c$. Then the mean width $\overline{\Delta\nu}$ of the state can be written

$$\overline{\Delta\nu} \sim \frac{1}{2\pi \tau_c} .$$

Thus if $\overline{\Delta\nu}$ is identified with the half-width γ_c of the absorption line,

$$\gamma_c \sim \frac{1}{2\pi \tau_c} . \quad (7)$$

Again the half-width found from classical theory and expressed in Eq. (6) is of the same order of magnitude as the half-width approximated from quantum theory in Eq. (7).

III. RELATIVE BROADENING ABILITIES

To gain knowledge about the ability of a non-absorbing gas to broaden a spectral line through the collision process, it is necessary to express the mean number of collisions per second f_c , experienced by an absorbing or emitting molecule, in terms of known or measurable quantities. Then the half-width γ_c of the collision broadened line can be found from the relation $\gamma_c = f_c / 2\pi$.

If D is the sum of the optical collision diameters of two colliding molecules, then the number of collisions per second is said to be $\pi D^2 \bar{u} N$, where N is the number of molecules per unit volume and \bar{u} is the mean speed¹⁰ of the molecules given by

$$\bar{u} = \sqrt{\frac{8kT}{\pi\mu}}$$

The reduced mass μ of the colliding molecules of masses m_a and m_b is given by the relation

$$\mu = \frac{m_a m_b}{m_a + m_b}$$

The mean collision frequency becomes

$$f_c = \pi D^2 \cdot \sqrt{\frac{8kT}{\pi\mu}} \cdot N$$

and then the half-width γ_c can be written

$$\gamma_c = \frac{D^2}{2} \left(\frac{8kT}{\pi\mu} \right)^{\frac{1}{2}} N$$

In order to extend this expression to account for a mixture of molecules, it can be generally expressed

$$\gamma_c = \left(\frac{2kT}{\pi} \right)^{\frac{1}{2}} \sum_i N_i D_{ai}^2 \left[\frac{1}{\mu_{ai}} \right]^{\frac{1}{2}}, \quad (8)$$

where N_i is the number of molecules of the i -th type per unit volume, D_{ai} is the sum of the optical collision diameters of the absorbing molecule and a molecule of the i -th type, μ_{ai} is the reduced mass of the colliding pair.

If the gas consists only of a binary mixture of molecules able to absorb a and molecules able to broaden b, then Eq. (8) can be written

$$\gamma_c = \left(\frac{2kT}{\pi} \right)^{\frac{1}{2}} \left[N_a D_{aa}^2 \left(\frac{2}{M_a} \right)^{\frac{1}{2}} + N_b D_{ab}^2 \left(\frac{M_a + M_b}{M_a M_b} \right)^{\frac{1}{2}} \right].$$

In terms of partial pressures $P_a = N_a kT$ and $P_b = N_b kT$, γ_c can be expressed

$$\gamma_c = \left(\frac{2kT}{\pi} \right)^{\frac{1}{2}} D_{ab}^2 \left(\frac{M_a + M_b}{M_a M_b} \right)^{\frac{1}{2}} [B P_a + P_b], \quad (9)$$

where $B = [2M_b / (M_a + M_b)]^{\frac{1}{2}} (D_{aa} / D_{ab})^2$ represents the ratio of the line broadening ability of the absorbing gas molecule a to that of non-absorbing foreign gas b. The quantity $(B P_a + P_b)$ is called the effective pressure and is designated P_e .

It is customary to employ N_2 as a standard broadening gas. A foreign broadening coefficient F can be defined as the ratio of line broadening ability of a foreign gas to that of N_2 . Then the F value of N_2 is taken to be unity and, in analogy to the expression for B, the following equation for F can be written,

$$F = \left[\frac{(M_a + M_b) M_{N_2}}{(M_a + M_{N_2}) M_b} \right]^{\frac{1}{2}} \frac{D_{ab}^2}{D_{a N_2}^2}. \quad (10)$$

The quantities F and B are useful since from them optical collision diameters D and line half-widths γ_c can be calculated. Measured values for F and B must be based on experimentally measurable quantities.

The measured absorbance $A_m(\nu)$ is different from the actual absorbance $A(\nu)$ because, for most existing spectrographs, the spectral slitwidth is much larger than the half-width of infrared absorption lines. Hence, sufficient resolution is lacking and it is not possible to make direct use of Lambert's law to find $A(\nu)$.

Theoretical considerations and experimental results^{11,12} indicate that the relation

$$\int_0^{\infty} A_m(\nu) d\nu = \int_0^{\infty} A(\nu) d\nu, \quad (11)$$

is valid for absorptances $A_m(\nu)$ and $A(\nu)$ associated with a single spectral line. The total absorptance $\int A(\nu) d\nu$ of a Lorentz line can be expressed¹³ in terms of line strength S , half-width γ , and sample thickness l by the expression

$$\int_0^{\infty} A(\nu) d\nu = 2\pi\gamma L(x), \quad (12)$$

where $L(x)$ is called the Ladenberg function with argument

$$x = \frac{Snl}{2\pi\gamma} \quad (13)$$

Two approximations¹⁴, referred to as the strong-line approximation and the weak-line approximation, reduce the Ladenberg expression to simple forms.

The strong-line approximation is valid when the spectral absorptance near the centers of the strongest lines is so great that an increase in absorber thickness nl or effective pressure P_e only results in increased spectral absorptance in the wings of the lines. In this approximation

$Snl/2\pi\gamma \gg 1$ and $L(x)$ converges to $(Snl/\pi^2\gamma)^{1/2}$. Then Eq. (12) can be written

$$\int_0^{\infty} A(\nu) d\nu = 2(Snl\gamma)^{1/2}. \quad (14)$$

Values of the effective pressure and absorber thickness for which the approximation is valid are said to be in the "square root" region of the curve of growth of the line.

The weak-line approximation is valid when the spectral absorptance is small at all frequencies. For this case, $Snl/2\pi\gamma \ll 1$ and $L(x)$ reduces to $(Snl/\pi^2\gamma)$; thus

$$\int_0^{\infty} A(\nu) d\nu = \frac{2Snl}{\pi}. \quad (15)$$

In the present study, the measured total absorptance $\int A_m(v)dv$ for an individual line was itself not measured directly. The averaging property of the spectrograph's finite slitwidth allows the integrated absorptance in a finite interval Δv between v and $v+\Delta v$ to become

$$\int_v^{v+\Delta v} A_m(v) dv = \overline{A_m(v)} \cdot \Delta v, \quad (16)$$

where $\overline{A_m(v)}$ is the fractional absorptance measured at the line center when the rectangular slitwidth is Δv . This expression is valid when the slit-width $\Delta v \gg \gamma$ and when $Sn\ell/2\pi\gamma \gg 1$; i.e., when values of P_e and $n\ell$ are in the "square root" region.¹⁵ Under these conditions, it can be assumed that $\overline{A_m(v)} \propto \int_0^\infty A(v) dv$.

Equation (14) implies that lines of equal absorptance measured from two samples of equal absorber thickness have equal half-widths; it follows that a comparison of half-widths at equal absorber concentration need only involve a comparison of measured absorptances $\overline{A_m(v)}$. Furthermore, from Eq. (9) it can be seen that the effective pressures P_e of two samples are equal when their line half-widths γ_e are equal. Thus an experimental determination of B at a given temperature would involve measurement of the average absorptance by gases in sample cells of different length in which the absorber thicknesses are the same. Then

$$B P_a^s + P_b^s = B P_a^\ell + P_b^\ell,$$

where the superscripts s and ℓ represent the short and long cells, respectively. Hence the expression for B is

$$B = \frac{P_b^\ell - P_b^s}{P_a^s - P_a^\ell}.$$

On the other hand, the foreign broadening coefficient F of non-absorbing gas b can be found by comparing the partial pressures required to produce

equal average absorptance when the two gases b and N_2 are added to equal samples of an absorbing gas. Thus the expression for F is defined as

$$F = \frac{P_{N_2}}{P_b} .$$

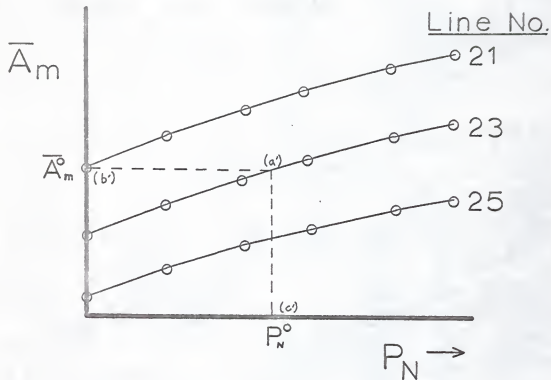
IV. REVIEW OF PREVIOUS WORK

Crane-Robinson and Thompson¹⁶ have measured the line half-widths for the fundamental vibration-rotation band of carbon monoxide broadened by various gases and have noted large differences between half-widths in different parts of the band. This prompted Draegert and Williams¹⁷ to investigate F values for individual lines in the CO fundamental, since measurements of the ratios of broadening abilities might be expected to give additional information regarding differences between various broadeners.

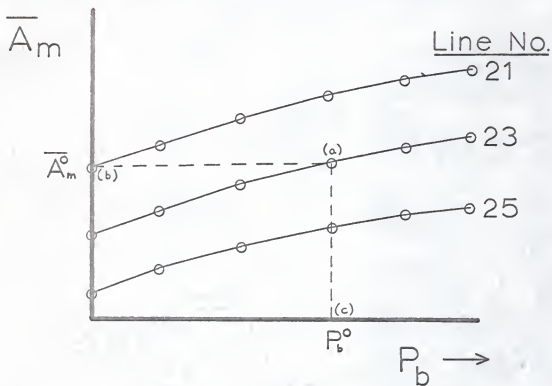
The technique used by Draegert and Williams for obtaining data on broadening abilities involved comparing average absorptances with associated partial pressures. To determine F values from the average absorptance, they introduced a small quantity of absorbing gas at partial pressure P_a into an absorption cell with a path length of 10 cm. Absorptance for the pure absorber and the progressively greater values of absorptance as nitrogen was added were measured. Curves of growth were plotted, giving absorptance at line centers as a function of nitrogen partial pressures. The process was repeated for the same quantity of broadening gas but with a broadening gas b other than nitrogen. Finally, recording appropriate values of P_b and P_N , for equal A_m , from the curves of growth as illustrated in Fig. 9, they found the foreign broadening coefficient F from the relation $F = P_w / P_b$.

Good results were obtained with an absorber concentration $n \ell \approx P_a \ell$ somewhat less than 1000 mm Hg cm. The broadening gas was added six or seven times to give a final total pressure near an atmosphere. This procedure produce average absorptance increases near 10 - 15% for each addition, an easily measured amount providing the average absorptance of pure absorber was at least 10 - 15 percent. The gas pressures and cell length were such

Figure 9. Typical curves of growth. The top curves represent A_m versus P_N plots. The lower curves represent A_m versus P_b plots. F values were found from the relation $F = P_N/P_b$, where P_N and P_b were measured at equal average measured absorbance.



N_2 -Curves of Growth



b-Curves of Growth

that the samples were always in the "square root" region.

Draegert's results are summarized in Fig. 10 for H_2 and D_2 and in Fig. 11 for the noble gases. Line number m corresponds to $J+1$, where J is the rotational quantum number of the initial state. In Fig. 10 the increase of F with increasing m up to $m = 21$ indicates that H_2 and D_2 are less effective than N_2 is in broadening CO lines near the band center, but more effective than N_2 in broadening CO lines in the wings of the band.

The F values of noble gases for lines also in the high frequency branch of the CO fundamental are shown in Fig. 11. It was noted that, for monatomic and diatomic gases with molecular masses less than that of N_2 , the F values for lines in the band wings are greater than for lines near the band center. The opposite is true for monatomic gases with molecular masses greater than that of N_2 . Chai¹⁸, in a later study, reported the same trend.

In the same study, Draegert and Williams used their results for F together with Chai's results for B and values of $\gamma_{c_0, c_0}^{\circ}$ obtained by Hunt, Toth, and Plyler¹⁹ to determine half-widths $\gamma_{c_0, b}^{\circ}$ due to collisions between CO absorber molecules and broadener molecules b . The results of their computations are listed in Table I.

They noted that values of $\gamma_{c_0, b}^{\circ}$ for H_2 , D_2 , and He remain fairly constant over the entire nineteen lines. This lack of variation confirmed the observations of Crane-Robinson and Thompson.

Table I. Half-widths $\gamma_{ca,b}^*$ for lines in the CO fundamental. The various broadening gases b are listed at the top of the table. Values are in units of $0.01 \text{ cm}^{-1}/\text{atm}$.

line number m	CO	H ₂	D ₂	N ₂	He	Ne	Ar	Kr	Xe
1	8.77	7.49	6.45	8.12	4.79	3.91	7.04	7.48	8.93
2	8.31	7.15 ¹	6.34	7.76	4.68	3.85	6.65	6.94	8.00
3	7.85	7.00	6.30	7.21	4.66	3.74	6.14	6.46	7.30
4	7.45	6.93	6.15	6.84	4.64	3.58	5.69	5.92	6.80
5	7.13	7.00	6.10	6.55	4.60	3.54	5.34	5.56	6.39
6	6.92	6.95	6.05	6.32	4.58	3.49	5.08	5.20	6.00
7	6.73	6.92	6.00	6.12	4.55	3.44	4.85	4.91	5.66
8	6.60	6.90	5.95	6.02	4.55	3.44	4.72	4.72	5.47
9	6.48	6.90	5.92	5.94	4.55	3.46	4.63	4.56	5.29
10	6.38	6.87	5.90	5.84	4.61	3.45	4.56	4.50	5.13
11	6.28	6.86	5.87	5.76	4.67	3.45	4.46	4.43	4.98
12	6.20	6.90	5.85	5.72	4.68	3.42	4.44	4.34	4.85
13	6.12	6.95	5.84	5.66	4.66	3.39	4.38	4.25	4.73
14	6.04	6.90	5.83	5.60	4.71	3.33	4.35	4.19	4.65
15	5.95	6.78	5.83	5.51	4.70	3.26	4.31	4.14	4.57
16	5.86	6.82	5.78	5.45	4.69	3.22	4.23	4.07	4.52
17	5.77	6.84	5.74	5.38	4.67	3.18	4.14	4.00	4.50
18	5.66	6.81	5.76	5.24	4.68	3.20	4.07	3.90	4.37
19	5.56	6.74	5.75	5.10	4.69	3.13	4.00	3.79	4.24

Figure 10. Experimental F values of H₂ and D₂ for individual lines of the CO fundamental determined by Dräeger and Williams.

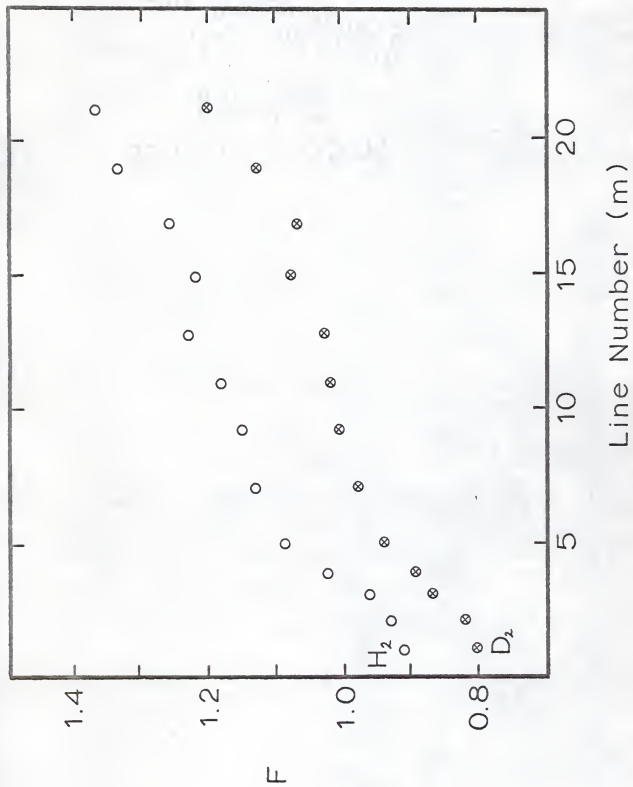
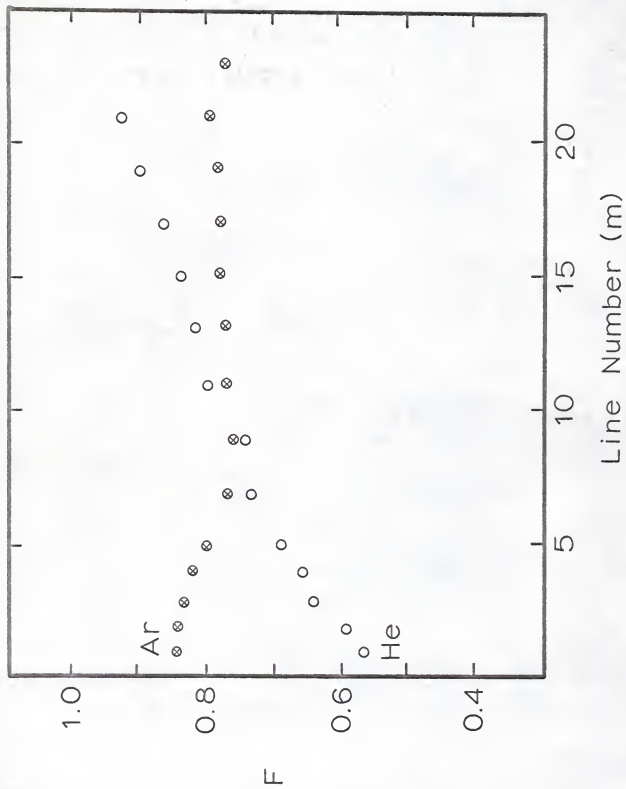




Figure 11. Experimental F values of Ar and He for individual lines of the CO fundamental determined by Draegert and Williams.



V. EXPERIMENTAL RESULTS

A. Problem for Investigation

The present study is an attempt to extend F value data into the high frequency wing of the carbon monoxide fundamental absorption band. This study involved measurement of the foreign gas broadening coefficient F from line 16 to line 30. Thus, since previous data went to line 21, overlap of the present data with the earlier provides an indication of consistency. The molecules studied for their broadening effects were He, D₂, H₂, and Ar.

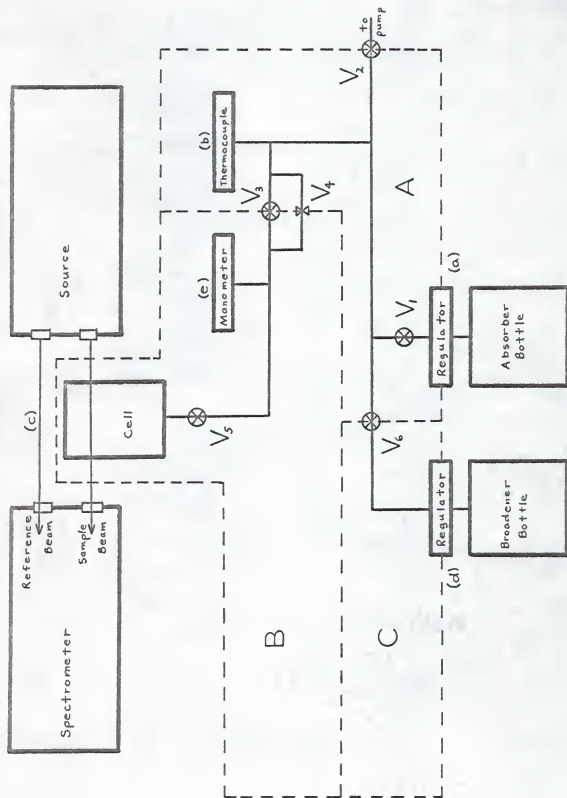
B. Description of Equipment and Experimental Procedure

A Perkin-Elmer Model 421 spectrometer was used for the entire study. This is a double-beam instrument which compares radiant flux from a reference beam to radiant flux from a sample beam; the sample beam passes through an absorption cell containing the gas samples. A plot of the resulting spectral absorbance as a function of frequency is recorded on the spectrometer's recording chart.

In order to achieve the "square root" region of the curve of growth for lines $m > 21$, for which the S values are small, it was necessary to use a larger absorption cell than the one used by Draegert. The absorption cell employed was a Perkin-Elmer multiple-traversal cell providing a path length of one meter. The cell was equipped with KBr windows and had a volume of 950 cm³.

To fill the absorption cell with the proper amount of gas, a copper and brass manifold assembly was employed with the necessary valves, regulators, and pressure gauges. Fig. 12 is a schematic diagram of the entire

Figure 12. A schematic diagram of the entire apparatus.



apparatus. A gas bottle of CO absorber was connected to a regulator at (a) which reduced the outflow pressure from the bottle to about 10 p.s.i. This regulator was connected to manifold valve V_1 through two feet of half-inch copper tubing. With the regulators at (a) and (d) closed but with all the remaining valves open, the entire manifold with connected gauges and cell was evacuated through valve V_2 to about 20μ Hg as determined by the thermocouple gauge at (b); then with valves V_2 , V_3 , V_4 , and V_6 closed, the regulator at (a) was opened so that section A of the manifold was pressurized to about 10 p.s.i. The pressure in section B could then be controlled by needle valve V_4 ; subsequently, section B of the manifold was filled to a CO pressure of approximately 30 cm Hg as measured with the mercury manometer at (e). With the regulator closed, valves V_2 and V_3 were opened to re-evacuate sections A and B to 20μ Hg in order to flush the system of impurities. After this initial flushing and evacuation of the manifold, the process was repeated as an added precaution.

After the second re-evacuation, valves V_2 , V_3 , and V_4 were closed and the manifold at (a) opened in order to pressurize section A to 10 p.s.i. Needle valve V_4 could then be used to allow a quantity of gas into manifold section B at the desired pressure. After the pressures in the cell at (c) and manometer at (e) had come to equilibrium, the manometer was read to a precision of 0.1 mm Hg. Glass stopcock valve V_5 on the cell was then closed and the spectrum of pure CO recorded.

Sections of the manifold A, C, and the part of B exclusive of the absorption cell were evacuated to 20μ Hg through V_2 . A foreign gas bottle was connected to the manifold through a regulator at (d). With valve V_5 closed, the manifold was flushed twice with broadening gas in the manner

previously described for the flushing with CO. With all parts of the manifold except the absorption cell evacuated to 20μ Hg, manifold sections C and A were pressurized to 10 p.s.i. The needle valve was then used to pressurize section B to a pressure greater than cell pressure. Valve V_5 was opened for three or four seconds to allow entry of broadening gas. Again the needle valve was used to pressurize section B above cell pressure; the foreign-gas admission process was repeated until the desired partial pressure of broadening gas was attained in the cell. To ensure equilibrium between cell and manometer, valve V_5 was opened several times; it was considered safe to leave the cell open for three or four seconds, since loss of absorber from the cell was insignificant in view of the large volume of the absorption cell, the much smaller volume of the manifold section between V_4 and V_5 , and the small 2 mm valve opening. This process was repeated until manometer readings stayed constant; then the cell pressure was recorded and the spectrum taken.

Additional broadening gas was added four more times with a similar sequence of events to increase the total pressure in the absorption cell, and a spectrum recording was taken for each pressure increase. A minimum of two minutes was allowed for the added gas to mix with the gas already in the cell. To ensure that this was enough time to prevent spectral discrepancies due to inadequate mixing time, a comparison of spectral recordings was made for different mixing times. Nitrogen broadening gas at a partial pressure of 100 mm Hg was added to CO absorbing gas at partial pressure 150 mm Hg; the spectrum was immediately recorded. Another spectrum of the same sample was recorded after allowing a 20 minute mixing time. No differences in the spectra were noted and, on this basis, it

was assumed that two minutes were sufficient to permit thorough mixing.

The absorber pressure to be obtained for use with all foreign broadening gases was required to match the absorber pressure used for N_2 ; thus, great care had to be exercised in metering CO into the cell. If the manometer was gently tapped at the same time CO gas was slowly introduced into the cell, it was found that the manometer was able to show an accurate CO pressure with little slowing of the manometer's response as a result of inertial and viscous effects. Otherwise, if gas was introduced too rapidly, the mercury tended to "climb" often as much as 0.5 mm after the needle valve was closed. This effect prevented good reproduction of CO absorber pressure.

As a test for the crucial requirement of equal CO pressure, initial spectral absorptances were compared. Measurements of various pure CO absorption peaks were made; if spectral absorptances for these peaks matched the spectral absorptances of CO peaks on corresponding lines of other spectra to plus or minus one percent, absorber pressures were well matched since associated F values were then reproducible.

Typical spectra of foreign gas broadened lines in the entire CO fundamental are shown in Fig. 13. Fig. 14 is an actual size tracing of typical spectra from the recording chart in the region of interest for the present study. This figure represents CO lines broadened by N_2 ; the CO absorber pressure is 241.5 mm Hg. To obtain these recordings, the spectrometer plotted spectral absorptance on the ordinate scale versus frequency on the abscissa. The lowest recording in this set represents the spectrum of pure CO; each succeeding spectrum corresponds to an increase in the partial pressure of broadening gas.

Figure 13. Typical spectra of foreign gas broadened lines in the entire CO fundamental.

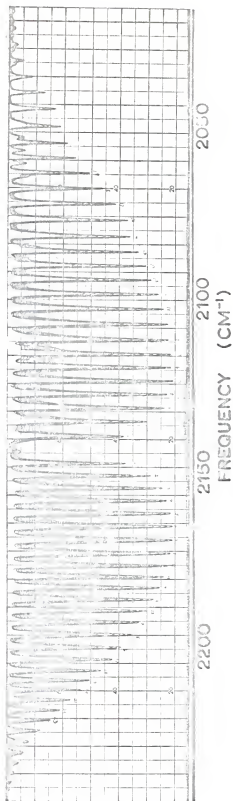
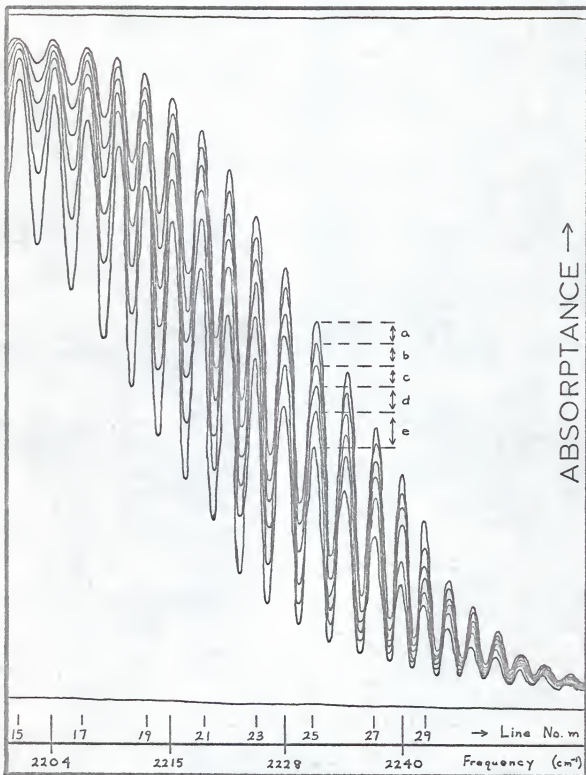


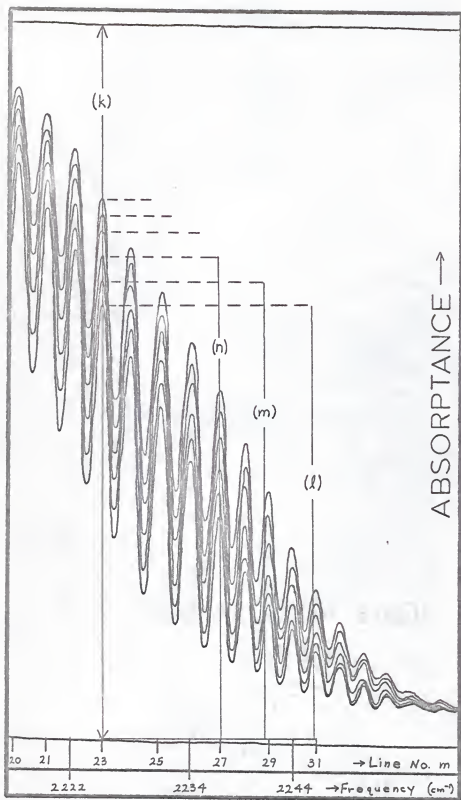
Figure 14. Actual size tracing of typical spectra from the recording chart for lines $m > 14$.



Two sets of spectra with different absorber pressures were needed to obtain lines with spectral absorptances $\overline{A}_m(\nu)$, which could be easily distinguished, and line strengths S , for which the strong-line approximation would be valid. For instance, in Fig. 14 the line strength S at $m = 15$ is great enough to allow the total absorptance to be given by the strong-line approximation. However, the spectral absorptances associated with line 15, shown in Fig. 14, are indistinguishable if we assume that each absorptance can only be determined by the spectrometer to ± 1.0 percent. On the other hand, at line $m = 25$ the spectral absorptances are well separated and clearly distinguishable as illustrated by letters a, b, c, etc., but it is probable that the line strength S associated with line $m = 25$ is too weak to allow the strong-line approximation to be valid. Hence, another set of spectra valid for lines $m > 24$ was needed. Figs. 14 and 15 illustrate the two sets of spectra used in this study; both were recorded with a spectral slitwidth of 1.5 cm^{-1} . Fig. 14 shows the first set, valid for lines $m = 16$ to 24; and Fig. 15 shows the second set, with a CO pressure of 340.3 mm Hg, valid for lines $m = 22$ to 28.

To reduce data from the spectrometer recording charts, a Gerber variable scale was used to measure the percentage of spectral absorptance at line centers. Fig. 15 illustrates how these percentages were measured for line $m = 23$ as a typical example. A variable scale was placed on the chart of recorded spectra and adjusted to represent the distance (k) as one hundred percent absorptance. Distances (l), (m), (n), etc. were then measured on the variable scale as percentages of distance (k); these percentages represented the spectral absorptance $\overline{A}_m(\nu)$ for each spectral absorptance increase. This process was repeated for all the desired lines in the band for both

Figure 15. Actual size tracing of typical spectra from the recording chart for lines $m > 19$.



nitrogen and foreign gas broadened spectra.

Curves of growth like those shown in Fig. 9 resulted when the values of $\overline{A_m(\nu)}$ on the ordinate scale were plotted versus the corresponding partial pressures of broadening gas on the abscissa scale. The sets of curves in Fig. 9 illustrate typical nitrogen and foreign gas curves of growth for lines 21, 23, and 25.

To calculate F values from the curves of growth, partial pressures of broadening gas were compared. On line 23, for example, a data point was selected as shown at (a) in Fig. 9; the corresponding absorptance $\overline{A_m}$ at (b) and partial pressure P_b^* at (c) were noted. To find the equivalent partial pressure P_w^* , the same absorptance $\overline{A_m}$ was marked on the ordinate scale at (b') and on line 23 at (a') of the N_2 curves of growth. Thus P_w^* was determined at (c'). The F value for this example was $F = P_w^*/P_b^*$. Approximately five such F values were determined for a given pair of lines. The average F value was used to represent the line.

C. Discussion of Results

Each set of foreign broadening coefficients F found for gases H_2 , Ar, D_2 , and He were first listed in Table II and then plotted in Figs. 16 - 19. A composite list of the most probable F values were then determined for the region of interest and listed in Table III; these F values were plotted in Figs. 20 - 23. Next, the present F values were compared with those of previous investigators; and finally the associated line half-widths were calculated and listed in Table IV.

Table II is a list of F values determined by the two sets of overlapping data. Along with the F values for each set are listed the associated mean deviations and the maximum estimated systematic error $\pm \Delta F_b$. The

Table II. F values for He, Ar, H₂, and D₂. The mean deviation is the average difference, without regard to sign, between five measured F values and the average F value for a line. The maximum estimated systematic error $\pm \Delta F$ is the uncertainty in the F value estimated from systematic error considerations.

Set I $P_{CO} = 241.5 \text{ mm Hg}$

m	F_{Ar}	mean deviation	$\pm \Delta F_{Ar}$	F_{He}	mean deviation	$\pm \Delta F_{He}$
16	.69	.06	.40	.86	.03	.38
17	.80	.06	.45	.91	.01	.52
18	.76	.02	.24	.85	.02	.33
19	.75	.02	.22	.85	.02	.24
20	.76	.02	.19	.90	.02	.22
21	.74	.01	.16	.88	.01	.19
22	.74	.02	.18	.89	.04	.16
23	.74	.02	.16	.84	.02	.16
24	.76	.02	.17	.89	.02	.18

m	F_{H_2}	mean deviation	$\pm \Delta F_{H_2}$	F_{D_2}	mean deviation	$\pm \Delta F_{D_2}$
16	1.22	.025	.88	.73	.07	.57
17	1.21	.05	.65	.89	.05	.50
18	1.18	.04	.43	.92	.05	.36
19	1.18	.03	.35	1.02	.02	.30
20	1.18	.06	.29	1.07	.01	.28
21	1.21	.04	.25	1.07	.03	.22
22	1.28	.03	.28	1.11	.05	.23
23	1.21	.02	.24	1.11	.04	.24
24	1.26	.01	.23	1.17	.03	.19

Table II. F values

Set II $P_{CO} = 340.3$ mm Hg

m	F_{Ar}	mean deviation	F_{Ar}	F_{He}	mean deviation	F_{He}
22	.69	.05	.20	.81	.04	.22
23	.78	.03	.25	.90	.05	.21
24	.71	.02	.22	.88	.03	.18
25	.72	.02	.23	.82	.05	.18
26	.80	.03	.37	.75	.05	.18
27	.80	.04	.28	.76	.08	.13
28	.79	.02	.23	.75	.12	.13

m	F_{H_2}	mean deviation	F_{H_2}	F_{D_2}	mean deviation	F_{D_2}
22	1.20	.02	.32	1.19	.06	.33
23	1.31	.03	.37	1.12	.04	.26
24	1.28	.02	.36	1.10	.04	.32
25	1.34	.03	.32	1.13	.03	.31
26	1.40	.03	.34	1.21	.04	.30
27	1.38	.06	.53	1.18	.05	.35
28	1.46	.04	.52	1.15	.04	.34

mean deviation of an F value is the average difference, without regard to sign, between each individual determination of the F value for that line and the average F value for the line; it is listed in the table to provide some idea of the consistency of the data. The maximum estimated systematic error $\pm \Delta F_s$ is the maximum uncertainty in each F value as determined from a reasonable estimate of systematic errors. A discussion of the errors of measurement is given in the Appendix.

The Figs. 16 - 19 show a plot of F values which start with line $m = 11$ and continue to line $m = 28$. Draeger's data are plotted in the region of lines $10 < m < 22$. The F values of Set I overlap Draeger's data and are plotted for lines $15 < m < 25$; the F values of Set II, in turn, overlap those in Set I and are plotted for lines in the region $21 < m < 29$. Error bars are drawn for F values in both Set I and Set II, where the shortest bars on each F value represent mean deviation and the long bars represent maximum estimated error. Though it was the original intention of this study to extend F value data to include lines $m = 29$ and 30 , this was not accomplished since the additional absorber thickness needed to apply the strong-line approximation to these lines would have required a third set of data with greatly increased absorber pressure and perhaps an even longer cell length.

Table III is a composite list of F values for lines $m = 16$ to 28 . These F values represent the best possible approximations available from the present data. They have a probable uncertainty no greater than ± 15 percent for lines $m = 26, 27$, and 28 far in the band wing, but nearer to a ± 10 percent uncertainty for the remaining lines listed. An explanation of the method used for determination of these F values and their probable

Figure 16. Experimental F values of H_2 for individual lines in the CO fundamental. Circles \circ represent data taken previously by Draeger. Squares \square represent data of Set I recorded for lines $m = 16$ to 24. Triangles \triangle represent data of Set II recorded for lines $m = 22$ to 28. Every F value plotted in this figure has two error bars; in each case the shorter error bar represents the mean deviation and the longer error bar represents the maximum estimated error.

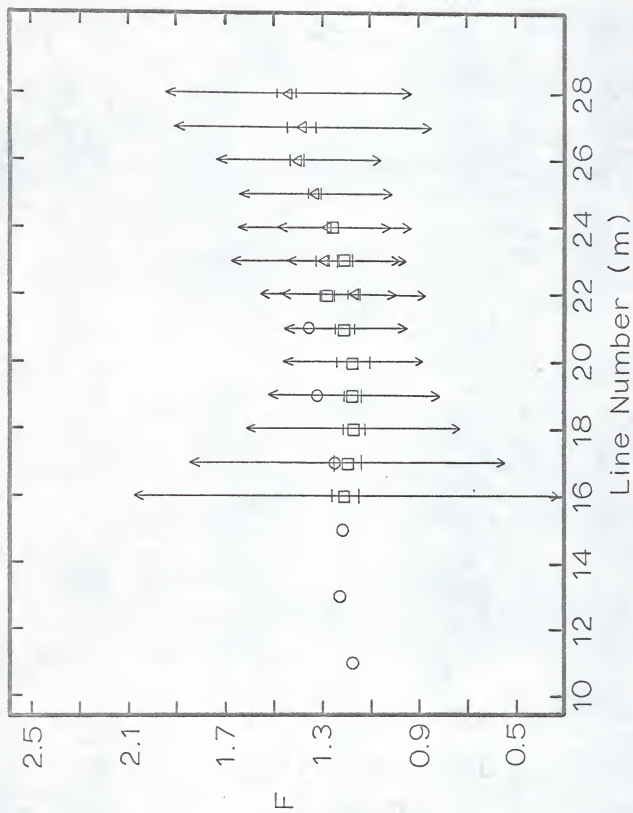


Figure 17. Experimental F values for D_2 for individual lines in the CO fundamental. Circles \circ represent data taken earlier by Draegert. Squares \square represent data of Set I recorded for lines $m = 16$ to 24. Triangles Δ represent data of Set II recorded for lines $m = 22$ to 28. Every F value plotted in this figure has two error bars; in each case the shorter error bar represents the mean deviation and the longer error bar represents the maximum estimated error.

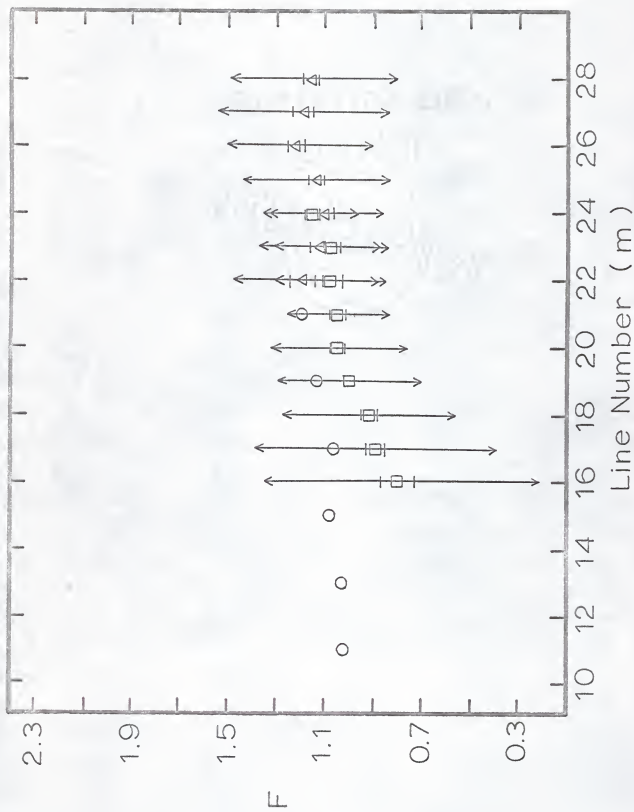


Figure 18. Experimental F values for He for individual lines in the CO fundamental. Circles O represent data taken earlier by Draeger. Squares \square represent data of Set I recorded for lines $m = 16$ to 24. Triangles Δ represent data of Set II recorded for lines $m = 22$ to 28. Every F value plotted in this figure has two error bars; in each case the shorter error bar represents the mean deviation and the longer error bar represents the maximum estimated error.

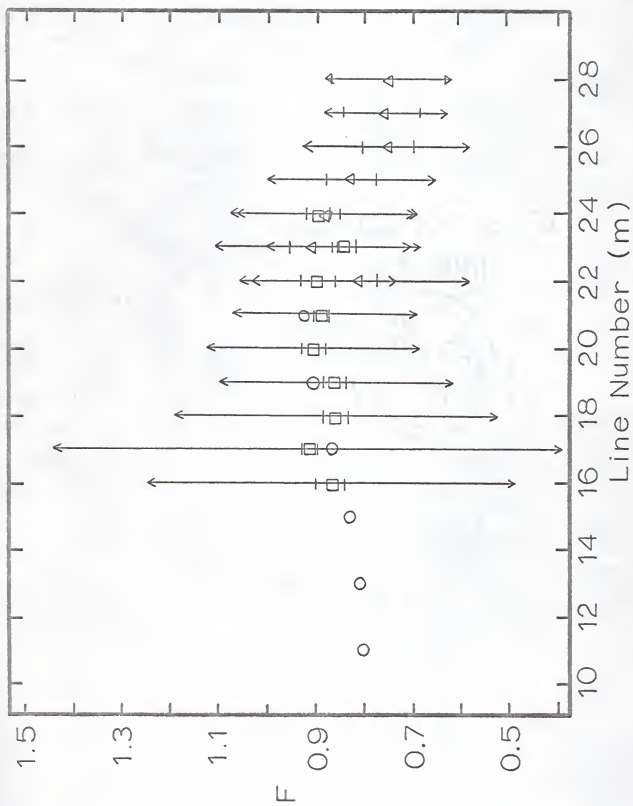


Figure 19. Experimental F values for Ar for individual lines in the CO fundamental. Circles O represent data taken earlier by Draeger. Squares □ represent data of Set I recorded for lines $m = 16$ to 24 . Triangles Δ represent data of Set II recorded for lines $m = 22$ to 28 . Every F value plotted in this figure has two error bars; in each case the shorter error bar represents the mean deviation and the longer error bar represents the maximum estimated error.

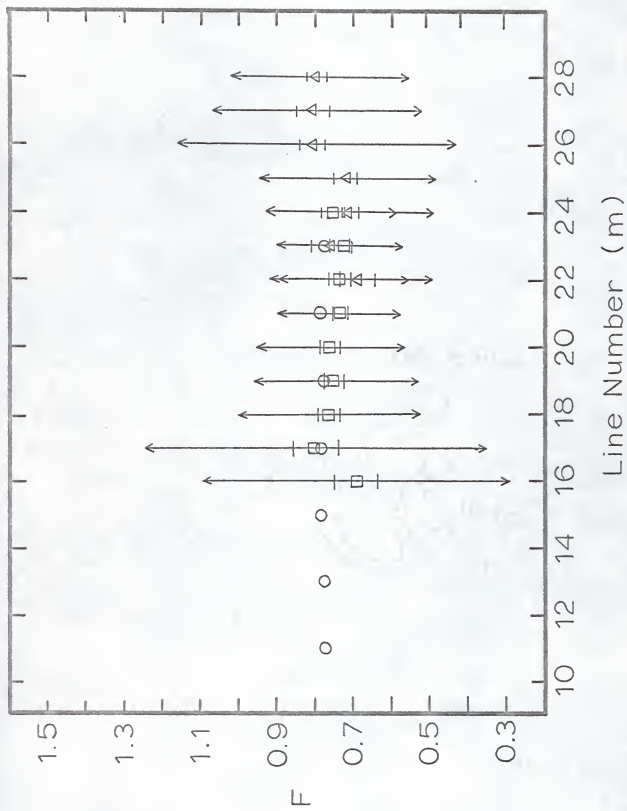


Table III. F values for lines $m = 16$ to 28. These F values represent the best estimates* of the correct F values that can be determined from the present data.

m	F_{H_2}	F_{D_2}	F_{Ar}	F_{He}
16	1.20	1.0	0.70	0.85
17	1.20	1.0	0.80	0.90
18	1.20	1.0	0.75	0.85
19	1.20	1.0	0.75	0.85
20	1.20	1.05	0.75	0.90
21	1.20	1.05	0.75	0.90
22	1.25	1.10	0.70	0.85
23	1.25	1.10	0.75	0.85
24	1.30	1.15	0.75	0.90
25	1.35	1.15	0.75	0.85
26	1.40	1.20	0.75	0.80
27	1.40	1.20	0.80	0.75
28	1.50	1.15	0.80	0.75

* The estimated uncertainty of F values for lines $m = 16$ to 25 is ± 10 percent, and ± 15 percent for the remaining lines.

uncertainties follows in the appendix.

Figs. 20 - 23 represent a plot of the values listed in Table III; these plots illustrate a similarity in the "trends" of the present data compared with that found in earlier studies. First, the trend of increasing F values with line number, noted by Draegert for diatomic gases with molecular masses less than that of N_2 , continues into the extreme wing. In Fig. 20 the hydrogen F value plot shows this continuation in the trend. The F values are greater than unity, indicating that H_2 is more effective in its ability to broaden CO spectral absorption lines than is N_2 for lines in the band region shown. Secondly, the D_2 data in Fig. 21 demonstrates that the F value increase with increasing m also continues into the wing of the CO absorption band. The F values, for the most part, are greater than unity, and thus D_2 is also a more effective broadening gas than is N_2 in the region shown. Third, F values for helium remain approximately constant as shown by Fig. 22. Draegert's F values for this monatomic gas increased with m to about line 17 where they began to level off to a constant value of about 0.9. The trend of constant F values continues into the extreme wing where they begin to decrease slightly starting at line $m = 26$. F values calculated for helium are all slightly less than unity; hence, helium is slightly less effective than N_2 in its ability to broaden CO spectral absorption lines. Finally, argon, the only broadening gas in the present study with a molecular weight greater than N_2 , again remains consistent with the trend of earlier data. Ar has associated F values plotted in Fig. 23. These F values, slightly less than unity, continue approximately constant into the extreme wing.

Figure 20. A plot of the F values of H_2 for lines $m = 16$ to 28.

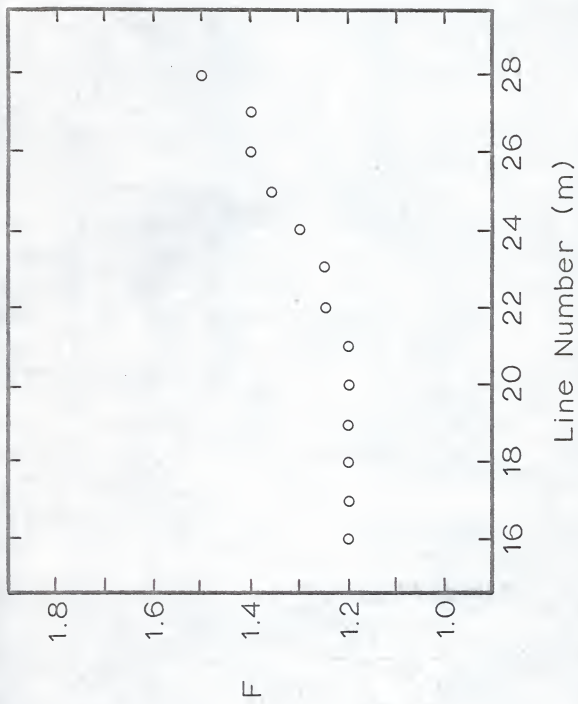


Figure 21. A plot of the F values of D_2 for lines $m = 16$ to 28.

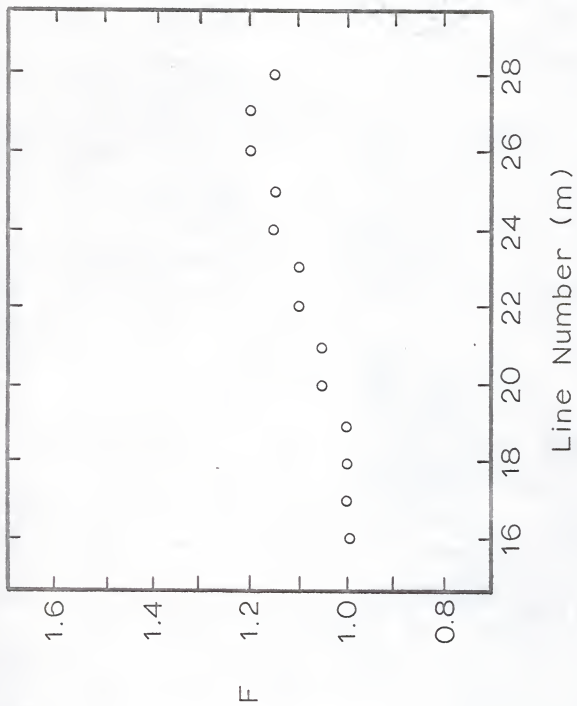


Figure 22. A plot of the F values of He for lines $m = 16$ to 28.

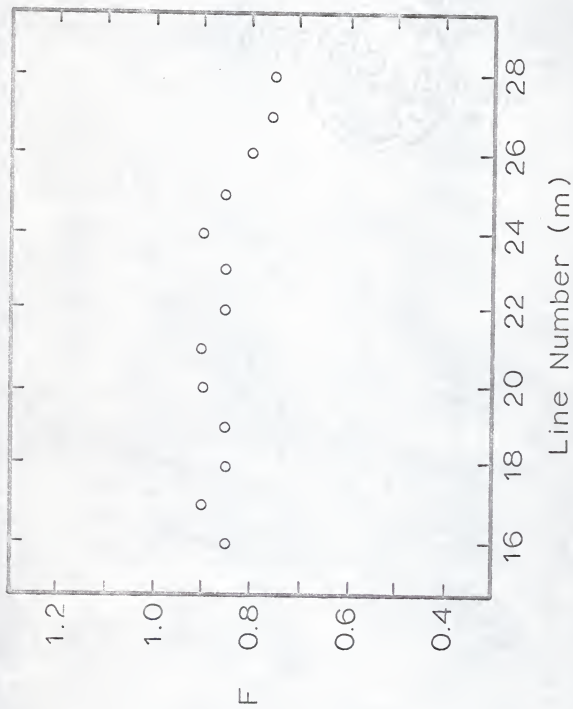
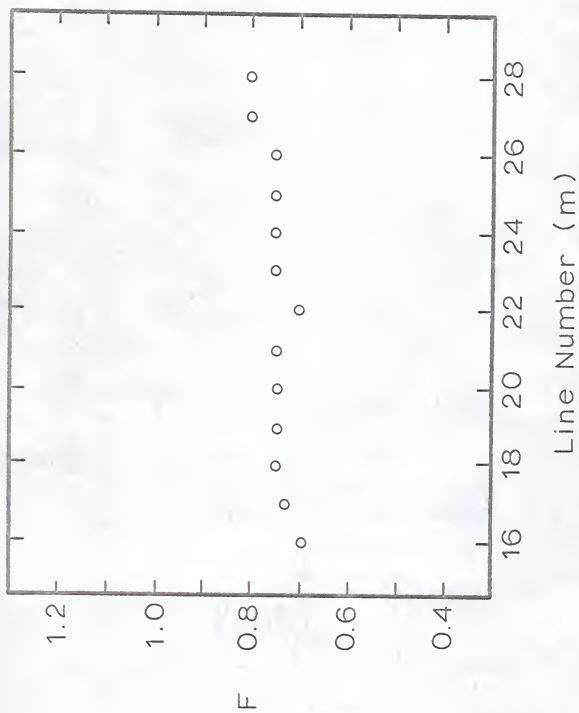


Figure 23. A plot of the F values of Ar for lines $m = 16$ to 28.



F-value data can be used in a determination of line half-widths. Half-widths of foreign gas broadened lines $\gamma_{co,b}^{\circ}$ can be related to half-widths of self-broadened lines $\gamma_{co,co}^{\circ}$. It follows from Eq. (9) that, at an effective pressure of one atmosphere, the ratio of half-widths $\gamma_{co,co}^{\circ}$, due to collisions between CO absorber molecules, to half-widths $\gamma_{co,b}^{\circ}$, due to collisions between CO absorber molecules and b broadener molecules, is given by the expression

$$\frac{\gamma_{co,co}^{\circ}}{\gamma_{co,b}^{\circ}} = \frac{D_{co,co}^{\circ}}{D_{co,b}^{\circ}} \left[\frac{2M_b}{M_{co} + M_b} \right]^{\frac{1}{2}} = B .$$

Hence, the relation between half-widths $\gamma_{co,co}^{\circ}$ and $\gamma_{co,b}^{\circ}$ is

$$\gamma_{co,b}^{\circ} = \gamma_{co,co}^{\circ} / B .$$

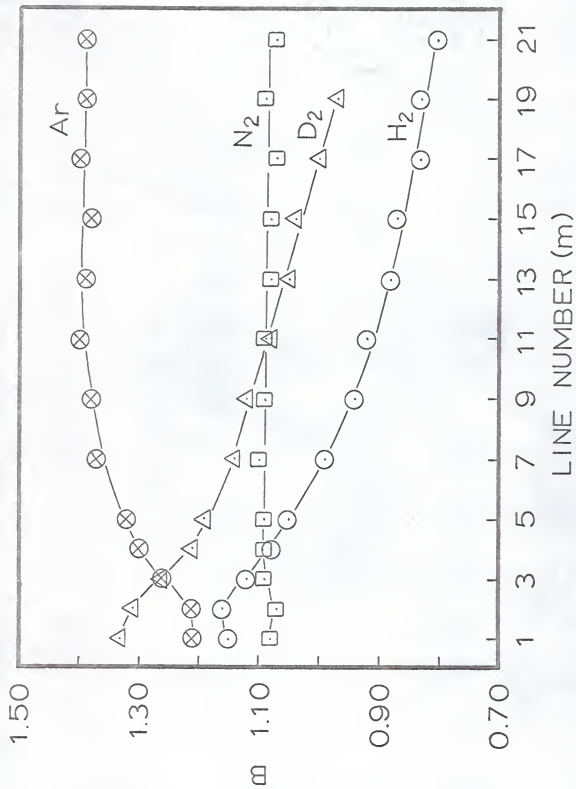
With use of the foreign broadening coefficient F this relation becomes

$$\gamma_{co,b}^{\circ} = F \left(\gamma_{co,co}^{\circ} / B_N \right) , \quad (17)$$

where B_N is the broadening ability of CO relative to N_2 .

With the previously measured values of $\gamma_{co,co}^{\circ}$ and B_N , together with the F value data of the present study, Eq. (17) was employed to calculate $\gamma_{co,b}^{\circ}$. Hunt, Toth, and Plyler¹⁹ have measured values of $\gamma_{co,co}^{\circ}$ for lines in the range $m = 1$ to $m = 31$. A. Chai²⁰ has determined B values for various broadening gases, including N_2 , for lines in the CO fundamental absorption band extending to $m = 21$. Plots of his B values are shown in Fig. 24. Chai found that B_N was approximately 1.08 for lines $m = 1$ to 21. G. Hoover²¹ obtained similar results in a later study for larger values of m . To employ Eq. (17) it was assumed that $B_N = 1.08$ for all of the lines; then the appropriate values of $\gamma_{co,co}^{\circ}$ from Table IV and F from Table III were used to calculate $\gamma_{co,b}^{\circ}$. Table IV is a list of the calculated

Figure 24. Chai's experimental B values for individual lines in the fundamental band of CO with respect to foreign gases Ar, N₂, D₂, and H₂.



half-widths over the range of lines $m = 16$ to 28.

Though these half-width results have a significant uncertainty, $\sim 15 - 20$ percent, it appears that the trends reported by earlier investigators continue into the extreme wing. Half-widths for H_2 , D_2 , and He are fairly constant over the 28 lines. This was the trend reported for lines nearer the band center, first by Crane-Robinson and Thompson, and later by Draegert and Williams. The trends of the Ar values are also essentially similar to those noted by the above investigators.

Table IV. Line half-widths* $\gamma_{\text{co,co}}^{\circ}$ and $\gamma_{\text{co,b}}^{\circ}$ in cm^{-1} at one atmosphere of pressure for lines $m = 16$ to 28. Values of $\gamma_{\text{co,co}}^{\circ}$ are those of Hunt, Toth, and Plyler.

m	$\gamma_{\text{co,co}}^{\circ}$	$\gamma_{\text{co,H}}^{\circ}$	$\gamma_{\text{co,O}}^{\circ}$	$\gamma_{\text{co,Nr}}^{\circ}$	$\gamma_{\text{co,Hc}}^{\circ}$
16	0.0586	0.065	0.054	0.038	0.046
17	.0577	.064	.053	.043	.048
18	.0566	.063	.052	.039	.045
19	.0556	.062	.052	.039	.044
20	.0545	.061	.053	.038	.045
21	.0535	.059	.052	.037	.045
22	.0525	.061	.053	.034	.041
23	.0515	.060	.052	.036	.041
24	.0504	.061	.054	.035	.042
25	.0494	.062	.053	.034	.039
26	.0484	.063	.054	.034	.036
27	.0474	.061	.053	.035	.033
28	.0465	.065	.050	.034	.032

* The estimated uncertainty of half-widths $\gamma_{\text{co,b}}^{\circ}$ for lines $m = 16$ to 25 is ± 15 percent and ± 20 percent for the remaining lines.

APPENDIX

A. Validity of Theoretical Assumptions and Approximations

The data in this study rest upon the validity of several assumptions and approximations to various derived relations. First, in Eq. (11) it was assumed that the total absorptance $\int A(v)dv$ for a line was equal to the total measured absorptance $\int A_m(v)dv$. The assumption was justified for the experimental procedures used in the present study. This assumption requires that the spectrum be scanned slowly enough to allow the recorder to follow the intensity of the radiant flux. Secondly, in Eq. (14) it was assumed that the strong-line approximation was valid. In this regard, great care was taken, as described in Chapter V, section B, to assure that F values were calculated for lines of sufficient strength to satisfy the necessary condition that $Sn\lambda/2\pi\gamma \gg 1$. Only those curves of growth which clearly demonstrated their "square root" dependency on broadening gas partial pressure were used. Finally, the approximation given by Eq. (16), requiring $\Delta v \gg \gamma$, was assumed valid since an examination of the data in Table IV indicates that the half-widths are indeed considerably smaller than the spectral slitwidth $\Delta v \sim 1.5 \text{ cm}^{-1}$. Therefore it can be assumed that any uncertainty in F value data obtained through these assumptions and approximations would be quite small.

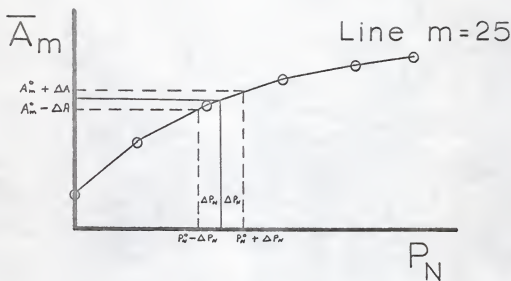
B. Sources and Treatment of Experimental Error

Among the sources of experimental error which include spectrometer recording accuracy, manometer error, absorption cell impurities, and errors in the data reduction process, by far the most significant contributor is the spectrometer's recording accuracy. The spectrometer's ability to

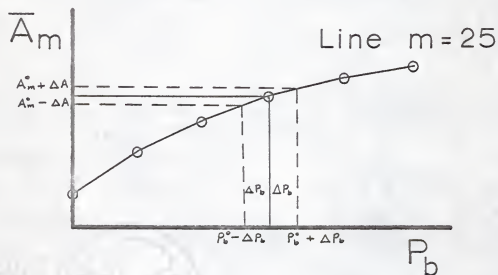
record the spectral absorptance $\overline{A}_m(\nu)$ accurately is limited by the instrument's reproducibility and noise level. Perkin-Elmer Corporation claims that the Model 421 is capable of reproducing a spectral recording to within ± 0.5 percent. A check with this instrument indicated that the claim was valid. Furthermore, to achieve the rapid response needed for high resolution, a high gain setting was used which introduced an additional uncertainty of ± 0.5 percent in the recorded spectrum. Thus the recorded absorptance peak \overline{A}_m for each line was uncertain by ± 1.0 percent of the full scale. The second source of experimental error was the manometer. The mercury manometer could be read to an accuracy of ± 0.2 mm Hg. However, considering that it was extremely unlikely for the manometer to be in perfect equilibrium with the absorption cell, and that viscous losses were to be had in the manometer, an uncertainty of ± 1.0 percent is a reasonable estimate of manometer accuracy. The change in peak absorptance due to this pressure uncertainty was too small to be detectable. Likewise, any effects of impurities in the absorption cell were insignificant; their effect had been reduced by obtaining a leak-tight manifold-cell assembly and by flushing the system repeatedly. Finally, errors introduced by the method of data reduction were not systematic and could be reduced by referring, where possible, to data points on the curves of growth as illustrated in Fig. 9. In general it was assumed that all sources of experimental error were quite small compared to the spectrometer's recording accuracy.

The maximum estimated errors of the F values listed in Table II were determined from a consideration of only the spectrometer's recording accuracy. The method of this determination is illustrated in Fig. 25. The top drawing in the figure is a typical curve of growth for nitrogen broadened CO

Figure 25. Illustration of how the uncertainty in spectral absorptance \bar{A}_m for a line produces a corresponding uncertainty in partial pressures P_N and P_b through the curve of growth.



N_2 -Curve of Growth



b-Curve of Growth

line $m = 25$. The bottom figure is a curve of growth for the same line when b was the broadening gas. To estimate the maximum error in the F value, a spectral absorptance A_m^0 was selected which corresponded to the average F value for the line. The corresponding pressures P_N^0 and P_b^0 could then be determined from the curves of growth. The spectral absorptance was uncertain by $\pm \Delta A$, which produced an uncertainty in the corresponding partial pressures of ΔP_N and ΔP_b as shown by the dashed lines in the figure. Then the maximum estimated error ΔF_b was defined as

$$\Delta F_b = \frac{P_N^0 + \Delta P_N}{P_b^0 - \Delta P_b} - \frac{P_N^0}{P_b^0} ;$$

the values for ΔF_b are listed in Table II.

While the maximum estimated error was quite large for many F values, it is probable that these F values are considerably closer to the correct value than the uncertainties shown in Figs. 17 - 20 would indicate. For instance, a comparison of the F values of the present study with earlier overlapping F values, as illustrated in Figs. 17 - 20, indicated that the F values match to within ± 10 percent and, in many cases, to ± 5 percent. Likewise, a comparison of the overlapping F values of Set I and Set II showed a general agreement to within ± 5.0 percent; very few overlapping F values differed by more than ± 10 percent. In addition, the mean deviation of each F value of Table II was generally less than ± 5.0 percent; if the magnitude of the spectrometer's recording inaccuracy was as large as it was assumed to be, a much longer mean deviation would have been expected. Thus the present data appear to be much more reliable than the listed uncertainties would indicate, since they are internally consistent and also consistent with the earlier data.

To determine a single F value for each line $m = 16$ to 28, it was

decided to weigh the F values in Table II according to the above considerations and to average overlapping values in order to obtain a "probable" F value for each line. This resulted in the F values listed in Table III and plotted in Figs. 21 - 24. These F values indicate the probable trends of broadening gases for lines in the extreme high frequency wing of the CO fundamental absorption band.

The uncertainties in the related line half-widths were approximately the sum of the uncertainties of F, $\gamma_{\text{co,co}}^{\circ}$, and B. The values of $\gamma_{\text{co,co}}^{\circ}$ found by Hunt, Toth, and Plyler were accurate enough to be considered exact. Chai's value for B was accurate to approximately ± 5.0 percent. Hence the uncertainty in the values for $\gamma_{\text{co,b}}^{\circ}$ was on the order of 15 percent for lines $m = 16$ to 25 and 20 percent for lines $m = 26, 27,$ and 28.

ACKNOWLEDGEMENT

The author gratefully acknowledges the assistance and patient guidance of Dr. Dudley Williams in the preparation of this manuscript. The author also wishes to express his appreciation to the National Science Foundation for providing financial assistance, and to Gary Hoover, Lloyd Tubbs, and David Wenstrand for their gracious help.

REFERENCES

1. G. Herzberg, Molecular Spectra and Molecular Structure, Vol. I: Spectra of Diatomic Molecules (2nd ed., New York: D. Van Nostrand Co., 1950), p. 112.
2. H. White, Introduction to Atomic Spectra, Vol. I (New York: McGraw-Hill Book Co., 1934), p. 421.
3. J. D. Jackson, Classical Electrodynamics, (New York: John Wiley and Sons, Inc., 1962), p. 601.
4. R. W. Ditchburn, Light, Vol. I (2nd ed., New York: Interscience Publishers, 1963), p. 93.
5. F. Reif, Fundamentals of Statistical and Thermal Physics, (New York: McGraw-Hill Book Co., 1965), p. 259.
6. Ditchburn, op. cit., p. 97.
7. W. Heitler, Quantum Theory of Radiation, (2nd ed., London: Oxford University Press, 1944), p. 61.
8. Reif, op. cit., p. 258.
9. C. H. Townes and A. L. Schalow, Microwave Spectroscopy, (New York: McGraw-Hill Book Co., 1955), p. 349.
10. Reif, op. cit., p. 268.
11. W. S. Benedict, et al., "The Strengths, Widths, and Shapes of Infrared Lines, Part I: General Considerations," The Canadian Journal of Physics, 34, 387 (1956).
12. W. S. Benedict, et al., loc. cit., "Part II: The HCl Fundamental," p. 855.
13. R. Lardenberg and F. Reiche, Ann. Physik 42, 181 (1913).
14. L. D. Kaplan and D. F. Eggers, J. Chem. Phys. 25, 876 (1956).
15. C. Crane-Robinson and H. W. Thompson, Proc. Roy. Soc. London A 272, 442 (1963).
16. Ibid.
17. D. Draegert and D. Williams, J. Opt. Soc. Am. To appear in the October issue, (1968).

18. A. Chai and D. Williams, J. Opt. Soc. Am. To appear in the October issue, (1968).
19. Professor Plyler, Private communication.
20. Chai and Williams, op. cit.
21. G. Hoover, Private communication.

FOREIGN GAS BROADENING OF LINES
IN THE WINGS OF THE CO FUNDAMENTAL

by

DAVID EDWARD SCHMIEDER

B.S., Wisconsin State University - Platteville, 1967

AN ABSTRACT OF A MASTER'S THESIS
submitted in partial fulfillment of the

requirements for the degree

MASTER OF SCIENCE

Department of Physics

KANSAS STATE UNIVERSITY

Manhattan, Kansas
1969

Certain polyatomic gases found in the atmosphere strongly absorb in the infrared region of the electromagnetic spectrum. Other atmospheric constituents, such as H_2 , N_2 , O_2 , and D_2 , as well as the noble gases, do not absorb in the infrared, but influence the ability of such gases as CO , CO_2 , and CH_4 to absorb. Absorption, or "line broadening" in the infrared spectra of gases, is mainly the result of collisions between molecules. The broadening abilities of different absorbing and non-absorbing gases are compared by the self-broadening coefficient $B(\nu)$, defined as the ratio of the line broadening ability of the absorbing gas at frequency ν to that of a foreign gas, and by the foreign gas broadening coefficient $F(\nu)$ defined as the ratio of the line broadening ability of a foreign gas to that of nitrogen gas at frequency ν . Earlier studies to determine F values for gases which included the broadening gases He, Ar, H_2 , and D_2 had found that F increased with rotational quantum number $J+1$ for He, D_2 , and H_2 broadened CO lines and that F values for Ar broadened CO lines remained approximately constant. While He and Ar were found to be generally less effective than N_2 in broadening CO lines, H_2 and D_2 were only less effective than N_2 near the band center but more effective than N_2 in broadening CO lines in the wings of the band. It was noted that, for monatomic and diatomic gases with molecular masses less than that of N_2 , the F values for lines in the band wings were greater than for lines near the band center; the opposite was true for monatomic gases with molecular masses greater than that of N_2 .

The present study extended the F value data for Ar, He, D_2 , and H_2 to line $J+1 = 28$ in the high frequency wing of the CO fundamental band. It was found that the trends noted for foreign gas broadened CO lines nearer

the band center continued into the extreme wing. Line half-widths were calculated from the F value data and again it was noted that the trends reported earlier continued into the extreme wing.